Characterization of mesothelioma and tissues present in contrast-enhanced thoracic CT scans

Neal Corson, William F. Sensakovic, Christopher Straus, Adam Starkey, and Samuel G. Armato III[a)]
Department of Radiology, The University of Chicago, 5841 South Maryland Avenue, Chicago, Illinois 60637

(Received 21 May 2010; revised 16 December 2010; accepted for publication 18 December 2010; published 28 January 2011)

Purpose: The purpose of this study was to characterize the Hounsfield unit (HU) distributions of mesothelioma and other tissues present in contrast-enhanced thoracic CT scans, to compare the HU distributions of mesothelioma, muscle, and liver by scanner and reconstruction filter/kernel combination, and to assess interpatient HU distribution variability.
Methods: The database consisted of 28 contrast-enhanced thoracic CT scans from different patients. For each scan, regions of interest were manually outlined within each of 13 tissues, including mesothelioma. For each tissue, the empirical percentiles in HU values were calculated along with the interpatient variability. The HU distributions of select tissues were compared across three different scanner and reconstruction filter/kernel combinations.
Results: The HU distributions of blood-containing tissues demonstrated substantial overlap, as did the HU distributions of pleural effusion, mesothelioma, muscle, and liver. The HU distribution of fat had the least overlap with the other tissues. Fat and muscle had the lowest interpatient HU variability and the narrowest HU distributions, while blood-containing tissues had the highest interpatient HU variability. A soft-tissue reconstruction filter/kernel yielded the narrowest HU distribution, and fat with artifact had the widest HU distribution.
Conclusions: Characterization of tissues in CT scans enhances the understanding of those tissues' HU distributions. Due to their overlapping HU distributions and close spatial proximity to one another, separating pleural effusion, mesothelioma, muscle, and liver from one another is a difficult task based on HU value thresholding alone. The results illustrate the wide distributions and large variability that exist for tissues present in clinical thoracic CT scans. [DOI: 10.1118/1.3537610]

Key words: Hounsfield units (HU), mesothelioma, tissue characterization, quantitative imaging, computer tomography (CT)

I. INTRODUCTION

Semiautomated and automated computer methods are proving useful in multiple medical imaging applications, such as screening, diagnosis, and therapeutic response assessment. While an understanding of the discrete information within images may not be necessary for the human visual system, computer algorithms utilize discrete information contained within images to perform their tasks. Thus, an understanding of this discrete information and its variability across different patients and imaging parameters is needed to improve computer methods. In computed tomography (CT), a CT section is made up of many pixels, each with its own discrete Hounsfield unit (HU) value. Tissue characterization captures the HU distribution of pixels for a given tissue.[1–15]

Many computer-aided diagnostic techniques for thoracic imaging require some level of image segmentation. The goal of the present study was to quantify the physical basis for difficulties encountered when a gray-level thresholding technique alone (which has been a common approach) is attempted for the purpose of segmenting tissues present within thoracic CT scans. Similar challenges may be encountered during the segmentation of thoracic structures for radiation therapy treatment planning. The present study sought to quantify the range (variability) of HU values for specific tissues and the extent of the overlap of these HU values for different, spatially adjacent tissues; these data are meant to serve as a guide for investigators engaged in image segmentation tasks.

The results from this study will further the understanding of HU distributions and variability contained within various tissues in thoracic CT scans. This understanding will prove beneficial when designing segmentation algorithms for thoracic CT scans.

II. MATERIALS AND METHODS

A database of 28 contrast-enhanced thoracic CT scans from 28 mesothelioma patients (23 male, 5 female, age 50–83 yr) was retrospectively collected and analyzed. The scans were performed at the University of Chicago Medical Center on three different CT scanners: Brilliance 16 ($n=2$), Brilliance 16P ($n=19$), and Brilliance 64 ($n=7$) (Philips Medical Systems, Cleveland, OH). Scans were acquired with 120 or 140 kVp and 113–330 mA s (mean: 237 mA s). All scans were infused with 120 ml of contrast agent (Omnipaque 350), according to a clinical imaging protocol that

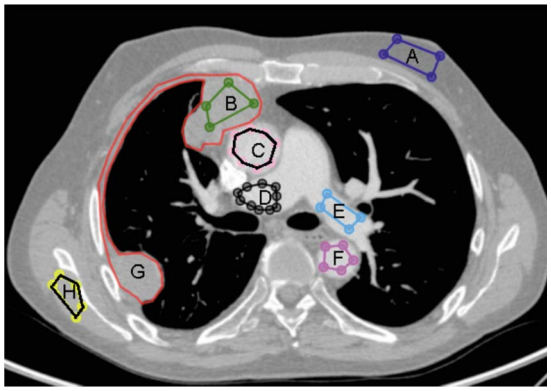

FIG. 1. ROIs selected from various tissues within the same CT section: (a) fat, (b) mesothelioma, (c) ascending aorta, (d) pulmonary artery with artifact, (e) pulmonary artery, (f) descending aorta, (g) mesothelioma contour by radiologist, and (h) muscle.

used an injection rate of 2.2 ml/s with a 65 s delay. All scans were reconstructed axially as 512×512 pixel images and had 1 mm reconstruction interval and 1 mm section thickness. The database was collected under an Institutional Review Board-approved protocol. All applicable Health Insurance Portability and Accountability Act regulations were observed during the collection, maintenance, and use of this database.

TABLE I. Number of scans, number of ROIs, and average number of pixels per ROI for each tissue type. AscAorta=ascending aorta, DescAorta =descending aorta, PA=pulmonary artery, PaArtifact=pulmonary artery with artifact, IVC=inferior vena cava, Effusion=pleural effusion, Meso =mesothelioma.

Tissue type	No. of scans	No. of ROIs	Average No. of pixels per ROI
Heart	28	84	6020
AscAorta	28	84	713
DescAorta	28	84	397
PA	28	84	472
PaArtifact	26	78	331
IVC	26	76	340
Effusion	10	28	1205
Meso	25	86	664
Muscle	28	84	567
Spleen	28	84	1559
Liver	28	84	2934
Fat	28	84	890
Fat Artifact	28	82	169

The 13 tissue types investigated were heart, ascending aorta, descending aorta, pulmonary artery, pulmonary artery with artifact, inferior vena cava (IVC), pleural effusion, mesothelioma, muscle, spleen, liver, fat, and fat with artifact,

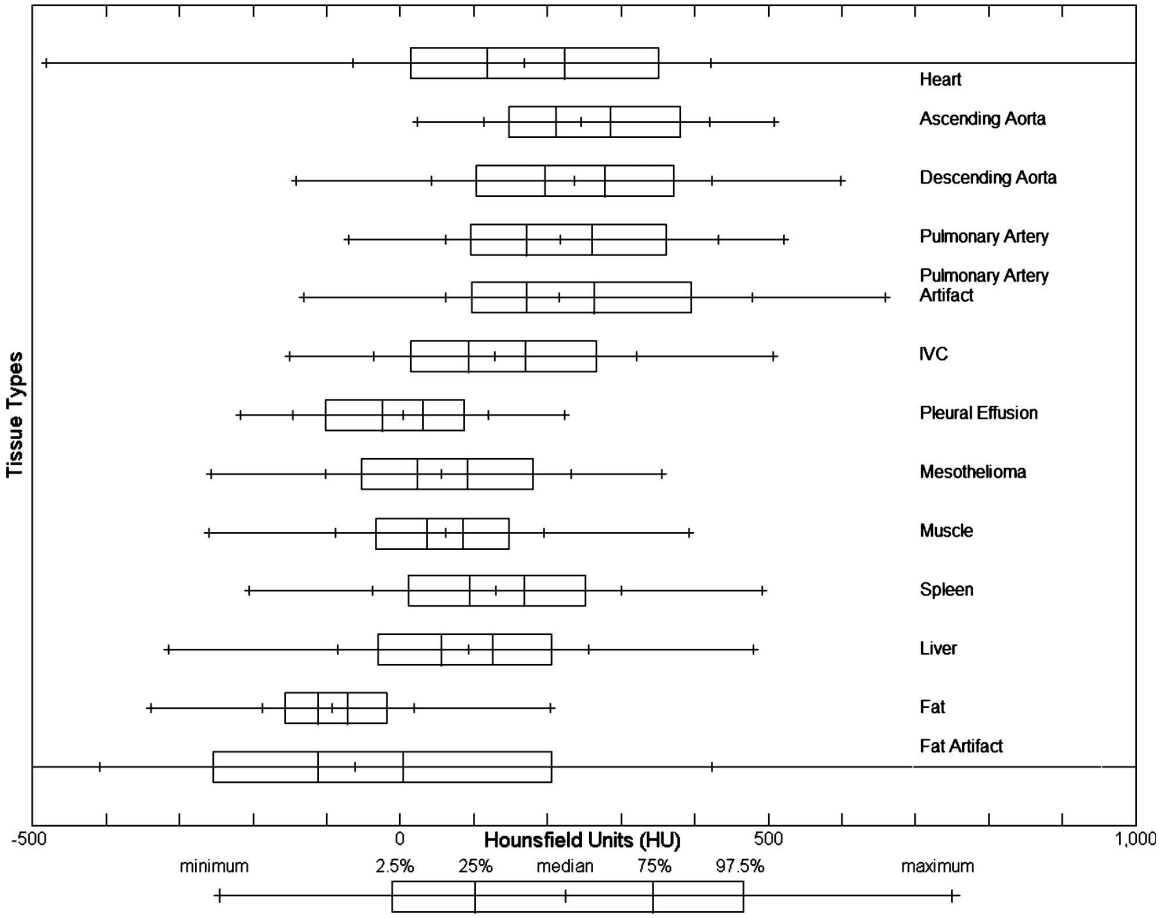

FIG. 2. The distributions of HU values for the 13 tissue types across all 28 CT scans. Extensive overlap exists among mesothelioma, muscle, and liver.

TABLE II. Statistics for HU distributions for different tissues across all 28 CT scans. AscAorta=ascending aorta, DescAorta=descending aorta, PA=pulmonary artery, PaArtifact=pulmonary artery with artifact, IVC=inferior vena cava, Effusion=pleural effusion, Meso=mesothelioma.

	Emprical percentiles (HU)							Percentile differences		Interpatient variability
Tissue type	Min	2.5%	25%	Median	75%	97.5%	Max	25%–75%	2.5%–97.5%	SD of medians
Heart	−482	14	118	169	223	351	1908	105	337	36
AscAorta	23	147	211	246	286	381	508	75	234	47
DescAorta	−142	103	197	236	278	372	598	81	269	41
PA	−71	95	172	218	261	362	521	89	267	60
PaArtifact	−132	97	171	216	263	396	659	92	299	56
IVC	−150	14	92	129	170	267	506	78	253	30
Effusion	−217	−102	−24	4	30	87	224	54	189	41
Meso	−258	−52	23	56	91	181	355	68	233	26
Muscle	−260	−33	37	61	85	147	393	48	180	7
Spleen	−205	11	94	130	168	252	492	74	241	25
Liver	−315	−31	56	92	126	205	480	70	236	23
Fat	−339	−156	−112	−93	−72	−19	204	40	137	11
Fat Artifact	−1000	−254	−112	−61	3	205	1545	115	459	38

where "artifact" refers to photon starving artifact due to contrast agent. An in-house image viewer and measurement system was used to manually construct and label the regions of interest (ROIs) within these 13 tissues. The ROIs (Fig. 1) were created away from the edges of tissues to avoid pixels found near tissue boundaries where partial volume effects occur. The ROIs were created by a single observer [NC] according to guidelines to ensure proper sampling of the sections and tissues within each section.

To compare the HU distributions of different tissues, distributions for each tissue were created by combining all the HU values from the ROIs within that tissue across all sections of all CT scans. The minimum, maximum, and median HU values as well as the HU value at 2.5, 25, 50, 75, and 97.5 percentiles were calculated. Overlap among the HU distributions of different tissue types was illustrated with a box-and-whiskers plot. For each tissue type, the interpatient variability (expressed as the standard deviation of median HU values across patients) was calculated.

The influence of scanner and reconstruction filter/kernel combination on HU distributions was investigated. The ROIs of mesothelioma, muscle, and liver were compared across three different scanner and reconstruction filter/kernel combinations: 16P B/B, 16P D/D, and 64 D/D, where the "16P" and "64" refer to the number of rows in the detector. Reconstruction filter/kernel "B/B" indicates soft-tissue reconstruction, while "D/D" indicates bone reconstruction.

III. RESULTS

The number of scans, the number of ROIs, and the average number of pixels per ROI for each tissue are presented in Table I. Pulmonary artery with artifact, IVC, pleural effusion, and mesothelioma have fewer than 28 scans due to the limited presence of these tissues within the scans. The number of ROIs per tissue varies due to the presence of the tissue within a scan or the ability to create an ROI within the tissue. Figure 2 illustrates the overlap of the tissues' HU distributions. The minimum, maximum, and median HU values as well as the 2.5, 25, 50, 75, 97.5, and 99.5 percentiles are presented in Table II. The percentile differences, 25%–75% and 2.5%–97.5%, which describe the width of the distribution, and the interpatient variability are also presented in Table II.

For mesothelioma, muscle, and liver, the number of scans and the number of ROIs for each combination of scanner and reconstruction filter/kernel are presented in Table III. As illustrated in Fig. 3, reconstruction filter/kernel B/B has lower percentile differences than reconstruction filter/kernel D/D. The interpatient variability (expressed as the standard deviation of the median HU values across patients) for the different combinations of scanner and reconstruction filter/kernel 16P B/B, 16P D/D, and 64 D/D are presented in Table IV. For mesothelioma, the interpatient variability for 16P D/D and 64 D/D are high due to each having an outlier. When the outliers are removed, the interpatient variability for 16P D/D and 64 D/D are 13 HU and 13 HU, respectively.

IV. DISCUSSION

This study characterized the HU distributions of mesothelioma and other tissues found in contrast-enhanced thoracic

TABLE III. Number of scans and ROIs by scanner and reconstruction filter/kernel combination. Meso=mesothelioma.

Tissue type	Filter/kernel	No. of scans	No. of ROIs
Meso	16P B/B	6	18
	16P D/D	13	44
	64 D/D	7	18
Muscle	16P B/B	6	18
	16P D/D	13	39
	64 D/D	7	21
Liver	16P B/B	6	18
	16P D/D	13	39
	64 D/D	7	21

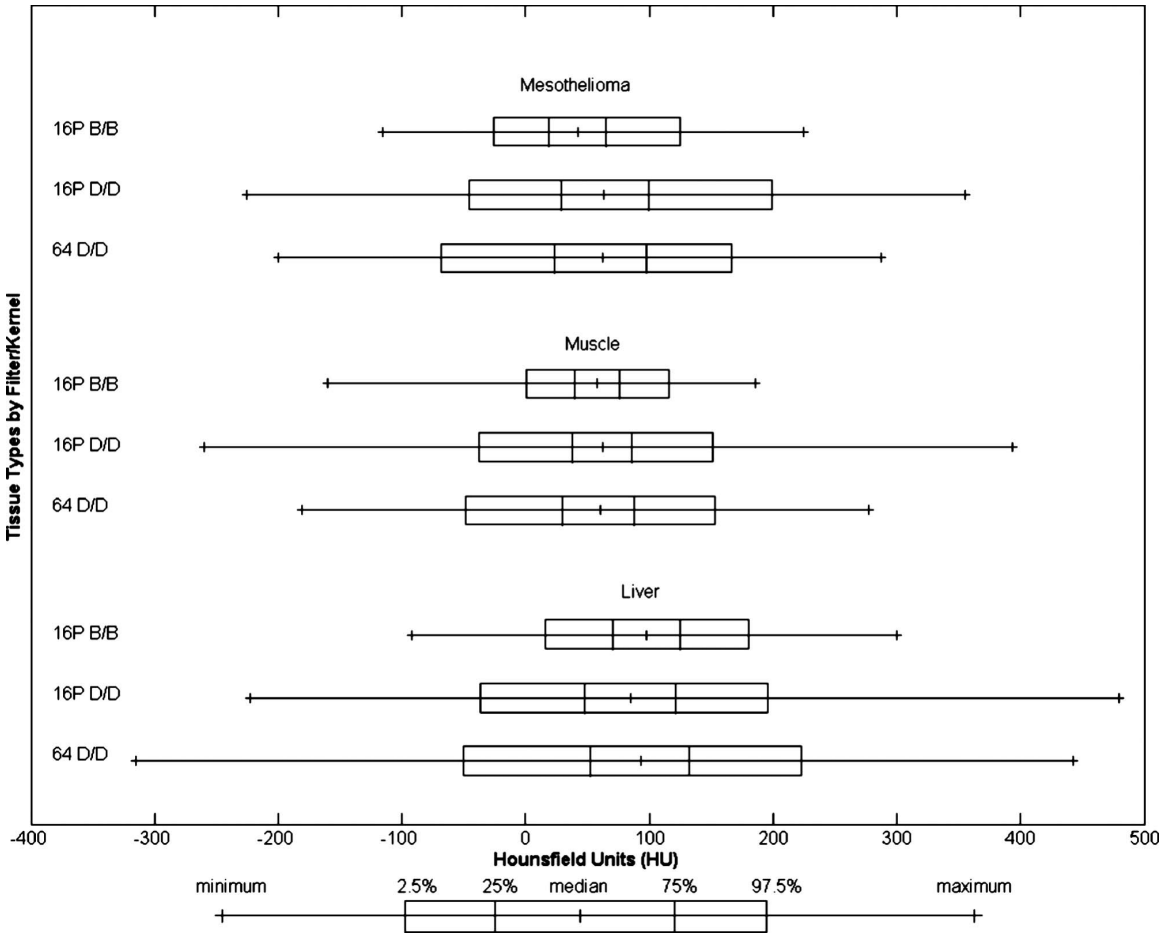

FIG. 3. The distributions of HU values of mesothelioma, muscle, and liver for three different scanner and reconstruction filter/kernel combinations.

CT scans of patients with mesothelioma. The purpose of the study was to investigate the aggregate variability of HU values for different tissues, with secondary evaluations of interpatient variability and variability due to different scanner and reconstruction filter/kernel combinations. The study did not evaluate the components of variability attributable to other image acquisition parameters. The results illustrate (1) large variability in the HU values within a specific tissue across patients in clinical thoracic CT scans acquired using the same imaging protocol on different scanners by the same manufacturer and (2) a large degree of overlap in the HU distributions of spatially adjacent structures.

The HU distributions of pleural effusion and mesothelioma overlap, as seen in Fig. 2. Such overlap makes sepa-

TABLE IV. HU statistics of mesothelioma, muscle, and liver by scanner and reconstruction filter/kernel combination. Meso=mesothelioma.

		Empirical percentiles (HU)							Percentile differences		Interpatient variability
Tissue type	Filter/kernel	Min	2.5%	25%	Median	75%	97.5%	Max	25%–75%	2.5%–97.5%	SD of medians
Meso	16P B/B	−116	−26	19	42	65	125	225	46	151	9
	16P D/D	−225	−46	29	63	99	199	355	70	245	33
	64 D/D	−200	−68	23	62	98	167	287	75	235	23
Muscle	16P B/B	−160	1	40	58	76	116	186	36	115	6
	16P D/D	−260	−38	38	62	86	151	393	48	189	8
	64 D/D	−181	−48	30	60	88	153	277	58	201	5
Liver	16P B/B	−92	16	70	98	125	180	300	55	164	23
	16P D/D	−223	−37	48	85	121	196	480	73	233	26
	64 D/D	−315	−50	52	93	132	223	442	80	273	18

ration of these structures based on HU values alone a difficult task. The HU distributions of mesothelioma, muscle, and liver overlap with the HU values of mesothelioma between pleural effusion (with lower HU values) and muscle and liver (with higher HU values). These similar distributions and similar anatomical locations make segmentation of mesothelioma, pleural effusion, liver, and muscle from one another a challenge. Segmentation algorithms that attempt to segment any of these four structures will require complex approaches beyond simple HU value thresholding. Fat, on the other hand, has the least overlap with the other distributions, as shown in Fig. 2. Thus, segmentation of fat from the other structures may be possible with simple thresholding-based segmentation techniques.[16]

For a given tissue, the interpatient variability (expressed as the standard deviation of the median HU values across patients) was calculated. Interpatient variability widens the HU distributions for each tissue across patients since, although the widths of tissue HU distributions for different patients were similar, the median values were shifted relative to those of other patients. A low interpatient variability demonstrates that the same tissue from different patients have similar median HU values. Muscle and fat exhibited the lowest interpatient variability.

When comparing distributions from different scanners and reconstruction filter/kernel combinations, mesothelioma, muscle, and liver were investigated because they are difficult to segment due to their similar HU values. As expected, the smoothing effect of the soft-tissue reconstruction filter/kernel B/B lowers the percentile differences across all three tissues when compared to D/D.

While the results and conclusions of this study are not surprising, a systematic investigation such as the one presented here is required to provide direct evidence of an otherwise expected finding. Many articles in the literature report algorithms that segment tissues through gray-level thresholding (simple thresholding as well as adaptive thresholding), and this study was intended to investigate the similarities of the gray levels depicted by various structures within thoracic CT scans in an effort to understand the reliability and generalizability of such approaches. Our findings suggest that segmentation of thoracic structures requires methods more complex than threshold-based segmentation alone.

We expected (1) large variability in the HU values within a specific structure across patients and scanners and (2) a large degree of overlap in the HU distributions of spatially adjacent structures. Both expectations are demonstrated in our results. These findings generate two key conclusions. First, that gray-level thresholding-based segmentation of structures in thoracic CT scans will likely prove challenging; second, that natural variability in these scans must be considered to provide segmentation algorithms with some element of generalizability. The essential finding from our study is not the absolute values of the HU distributions presented, but rather the range of HU values for specific tissues and the extent of the overlap of these HU ranges for different, spatially adjacent tissues.

Further research should investigate intrapatient variability, which would require multiple scans for the same patient. This study had a limited database of 28 patients; a similar study with a larger database would yield more robust results. While this study examined Philips scanners, future studies should include scans from multiple scanner manufacturers.

V. CONCLUSION

This study characterized tissues found within contrast-enhanced thoracic CT scans of mesothelioma patients. The HU values of mesothelioma tend to fall between those of pleural effusion (with lower HU values) and those of muscle and liver (with higher values). The similar HU values and close spatial proximity make computerized segmentation of these four structures based on HU values alone a challenge. Of the tissues investigated, fat has a narrow distribution, low interpatient variability, and limited overlap with other tissues, which make it an ideal candidate for threshold-based segmentation. The results illustrate the wide distributions and large variability that exist for tissues present in clinical thoracic CT scans acquired using the same imaging protocol on different scanners by the same manufacturer.

ACKNOWLEDGMENTS

The authors would like to thank Lorenzo Pesce, Ph.D., for many insightful and valuable conversations. This work was supported by USPHS under Grant No. CA102085.

[a]Author to whom correspondence should be addressed. Electronic mail: s-armato@uchicago.edu; Telephone: 773-834-3044; Fax: 773-702-0371.

[1]A. C. Best, A. M. Lynch, C. M. Bozic, D. Miller, G. K. Grunwald, and D. A. Lynch, "Quantitative CT indexes in idiopathic pulmonary fibrosis: Relationship with physiologic impairment," Radiology **228**, 407–414 (2003).

[2]A. C. Best, J. Meng, A. M. Lynch, C. M. Bozic, D. Miller, G. K. Grunwald, and D. A. Lynch, "Idiopathic pulmonary fibrosis: Physiologic tests, quantitative CT indexes, and CT visual scores as predictors of mortality," Radiology **246**, 935–940 (2008).

[3]M. J. Gilman, R. G. Laurens, Jr., J. W. Somogyi, and E. G. Honig, "CT attenuation values of lung density in sarcoidosis," J. Comput. Assist. Tomogr. **7**, 407–410 (1983).

[4]P. G. Hartley, J. R. Galvin, G. W. Hunninghake, J. A. Merchant, S. J. Yagla, S. B. Speakman, and D. A. Schwartz, "High-resolution CT-derived measures of lung density are valid indexes of interstitial lung disease," J. Appl. Physiol. **76**, 271–277 (1994).

[5]H. Sumikawa, T. Johkoh, S. Yamamoto, K. Takahei, T. Ueguchi, Y. Ogata, M. Matsumoto, Y. Fujita, J. Natsag, A. Inoue, M. Tsubamoto, N. Mihara, O. Honda, N. Tomiyama, S. Hamada, and H. Nakamura, "Quantitative analysis for computed tomography findings of various diffuse lung diseases using volume histogram analysis," J. Comput. Assist. Tomogr. **30**, 244–249 (2006).

[6]N. Sverzellati, M. Zompatori, G. De Luca, A. Chetta, C. Bna, F. Ormitti, and R. Cobelli, "Evaluation of quantitative CT indexes in idiopathic interstitial pneumonitis using a low-dose technique," Eur. J. Radiol. **56**, 370–375 (2005).

[7]T. Okada, S. Iwano, T. Ishigaki, T. Kitasaka, Y. Hirano, K. Mori, Y. Suenaga, and S. Naganawa, "Computer-aided diagnosis of lung cancer: Definition and detection of ground-glass opacity type of nodules by high-resolution computed tomography," Jpn. J. Radiol. **27**, 91–99 (2009).

[8]F. Pombo, E. Rodriguez, M. V. Caruncho, C. Villalva, and C. Crespo, "CT attenuation values and enhancing characteristics of thoracoabdominal lymphomatous adenopathies," J. Comput. Assist. Tomogr. **18**, 59–62 (1994).

[9]H. S. Park, J. M. Lee, S. H. Kim, J. Y. Jeong, Y. J. Kim, K. H. Lee, S. H. Choi, J. K. Han, and B. I. Choi, "CT differentiation of cholangiocarcinoma from periductal fibrosis in patients with hepatolithiasis," AJR, Am.

J. Roentgenol. **187**, 445–453 (2006).
[10]L. Sjostrom, H. Kvist, A. Cederblad, and U. Tylen, "Determination of total adipose tissue and body fat in women by computed tomography, 40K, and tritium," Am. J. Physiol. **250**, E736–45 (1986).
[11]C. Ricci, R. Longo, E. Gioulis, M. Bosco, P. Pollesello, F. Masutti, L. S. Croce, S. Paoletti, B. de Bernard, C. Tiribelli, and L. Dalla Palma, "Non-invasive in vivo quantitative assessment of fat content in human liver," J. Hepatol **27**, 108–113 (1997).
[12]T. Iida, S. Yagi, K. Taniguchi, T. Hori, S. Uemoto, K. Yamakado, and T. Shiraishi, "Significance of CT attenuation value in liver grafts following right lobe living-donor liver transplantation," Am. J. Transplant. **5**, 1076–1084 (2005).
[13]L. E. Davidson, J. L. Kuk, T. S. Church, and R. Ross, "Protocol for measurement of liver fat by computed tomography," J. Appl. Physiol. **100**, 864–868 (2006).
[14]K. R. Nandalur, A. H. Hardie, S. R. Bollampally, J. P. Parmar, and K. D. Hagspiel, "Accuracy of computed tomography attenuation values in the characterization of pleural fluid: An ROC study," Acad. Radiol. **12**, 987–991 (2005).
[15]K. S. Lee, J. G. Im, K. O. Choe, C. J. Kim, and B. H. Lee, "CT findings in benign fibrous mesothelioma of the pleura: Pathologic correlation in nine patients," AJR, Am. J. Roentgenol. **158**, 983–986 (1992).
[16]T. Yoshizumi, T. Nakamura, M. Yamane, A. H. Islam, M. Menju, K. Yamasaki, T. Arai, K. Kotani, T. Funahashi, S. Yamashita, and Y. Matsuzawa, "Abdominal fat: Standardized technique for measurement at CT," Radiology **211**, 283–286 (1999).